THE JOURNAL OF PHYSICAL CHEMISTRY A
A JOURNAL OF THE AMERICAN CHEMICAL SOCIETY

pubs.acs.org/JPCA

Article

Rate Coefficients for OH + NO (+N_2) in the Fall-off Regime and the Impact of Water Vapor

Published as part of The Journal of Physical Chemistry virtual special issue "Advances in Atmospheric Chemical and Physical Processes".

Wenyu Sun, Jos Lelieveld, and John N. Crowley*

Cite This: *J. Phys. Chem. A* 2022, 126, 3863−3872

Read Online

ACCESS | Metrics & More | Article Recommendations | Supporting Information

ABSTRACT: The termolecular, association reaction between OH and NO is a source of nitrous acid (HONO), an important atmospheric trace gas. Rate coefficients for the title reaction as recommended by evaluation panels differ substantially at the temperatures and pressures that prevail in the Earth's boundary layer where the reaction is in the fall-off regime between low- and high-pressure limiting rate coefficients. Using pulsed laser methods for generation and detection of OH, we have reinvestigated the kinetics of the title reaction at pressures of 22−743 Torr (1 Torr = 1.333 hPa) and temperatures (273, 298, and 333 K) in pure N_2 and in N_2−H_2O bath gases. In situ optical absorption measurements were used to rule out any bias due to NO_2 or HONO impurities. Our rate coefficients (k_1) in N_2 bath gas are parametrized in terms of low-pressure (k_0) and high-pressure (k_∞) rate coefficients and a fall-off parameter (F_C) with $k_{1,0}^{N_2} = 7.24 \times 10^{-31} (T/300\ \mathrm{K})^{-2.17}$ cm^6 molecule^{-2} s^{-1}, $k_{1,\infty} = 3.3 \times 10^{-12} (T/300\ \mathrm{K})^{-0.3}$ cm^3 molecule^{-1} s^{-1}, and $F_C = 0.53$. Used with the "Troe" expression for termolecular reactions, these parameters accurately reproduce the current data in the fall-off regime and also capture literature rate coefficients at extrapolated temperatures. The presence of water vapor was found to enhance the rate coefficients of the title reaction significantly. The low-pressure limiting rate coefficient in H_2O bath gas is a factor 5−6 larger than in N_2, at room temperature ($k_{1,0}^{H_2O} = 4.55 \times 10^{-30} (T/300\ \mathrm{K})^{-4.85}$ cm^6 molecule^{-2} s^{-1}) indicating that H_2O is much more efficient in quenching the association complex HONO* through collisional energy transfer. Based on measurements in N_2−H_2O mixtures, a parametrization of k_1 including both N_2 and H_2O as third-body quenchers was derived. Neglecting the effect of H_2O results, e.g., in an underestimation of k_1 by >10% in the tropical boundary layer.

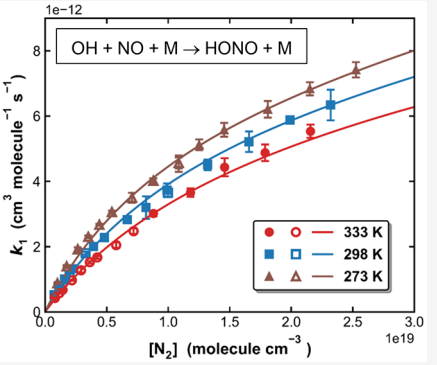

1. INTRODUCTION

Nitrogen monoxide (NO) is a short-lived intermediate involved in a variety of chemical reactions throughout the Earth's atmosphere,[1,2] where it is quickly oxidized to NO_2 by reaction with O_3,[3] peroxy radicals,[4] NO_3,[5] and halogen oxides.[6] During the day, NO_2 is rapidly photolyzed back to NO so that a photostationary state between NO and NO_2 evolves. NO and NO_2 are together referred to as NO_x, a critical component in the photochemical formation of ozone and smog in the lower atmosphere[1] and in the destruction of O_3 in the lower stratosphere.[7]

Both NO and NO_2 can also be oxidized by reaction with OH in termolecular reactions forming nitrous (HONO) and nitric acid (HNO_3):

$$\mathrm{NO + OH\ (+M) \rightarrow HONO\ (+M)} \quad \text{(R1)}$$

$$\mathrm{NO_2 + OH\ (+M) \rightarrow HNO_3/HOONO\ (+M)} \quad \text{(R2)}$$

During the daytime, HONO is photolyzed to OH + NO with a lifetime of ≥1 h[8] and may represent a significant source of OH in some environments, especially at sunrise. Apart from its formation in R1, additional sources of HONO include heterogeneous or photochemical reactions of NO_x and other reactive nitrogen compounds on various surfaces, emission from soil, and the photolysis of particulate nitrate.[9−11]

Termolecular reactions, which involve formation of an activated association complex whose relative rate of dissociation back to reactants and collisional quenching determine the effective rate coefficient, are pressure (and temperature) dependent. Such reactions often demonstrate "fall-off" behavior, and the Troe formalism[12] has been widely adopted to parametrize the rate coefficients in terms of high- and low-pressure limiting rate coefficients (k_∞ and k_0, respectively) and a broadening factor (F_C) to characterize the transition regime

Received: April 7, 2022
Revised: May 24, 2022
Published: June 8, 2022

in between. Recently, we presented measurements of rate coefficients for the termolecular reaction of OH with NO_2 and SO_2 under fall-off conditions at temperatures prevalent from the Earth's surface to the lower stratosphere.[13−15]

For the title reaction, several experimental data sets[16−32] were obtained from the 1970s to 1990s, mainly at low pressures in He and Ar bath gases to aid detection of OH. Although highly desirable for the purpose of deriving atmospherically relevant rate coefficients, data sets in N_2 at conditions relevant for the lower atmosphere (pressures up to 1 bar air) are sparse.[22,27,32]

Figure 1 presents a comparison between values of k_1 recommended by the IUPAC[33,34] and NASA[35] evaluation

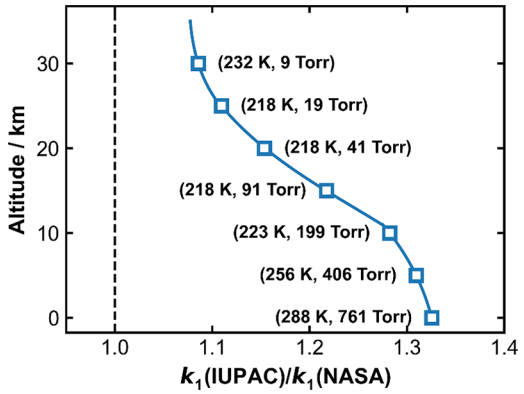

Figure 1. Ratio between rate coefficients, k_1, derived using the IUPAC and NASA parametrizations at different altitudes in the atmosphere. The pressures and temperatures at each altitude were calculated using parameters given in an Earth atmosphere model (https://www.grc.nasa.gov/www/BGH/atmosmet.html).

panels at different altitudes in the Earth's atmosphere (i.e., at different temperatures and pressures). The largest differences are seen for the lower atmosphere (especially in the planetary boundary layer), with better agreement in the stratosphere at low temperatures and pressures. IUPAC and NASA derived similar values of k_∞ (based on high-pressure measurements in He bath gas) and for k_0 based on different studies[19−22,24,26,27] in which N_2 was used as a third-body. To some extent, the different rate coefficients can thus be attributed to the broadening factors chosen: 0.6 by NASA and 0.81 by IUPAC.

Previous experimental work in different bath gases[18,19,21,22,25,36] elucidated the different collisional transfer efficiency of various third-body quenchers for the title reaction. In particular, H_2O was found to be a more efficient third-body than larger molecules with more vibrational degrees of freedom such as SiF_6 and CF_4.[22] The influence of H_2O on k_1 was also highlighted in a recent study,[37] which explored the role of water clusters at very low temperatures (60−135 K) in a Laval nozzle expansion. Our recent studies on the reactions of OH with NO_2 and SO_2[14,15] revealed that HNO_3/NO_2 and H_2SO_4/SO_2 ratios in some parts of the atmosphere could be significantly modified by the presence of H_2O.

The goals of this experimental work are 1) to quantify the impact of H_2O as a third-body quencher on the title reaction, 2) to derive accurate values of k_1 in the "fall-off" regime in N_2 bath gas, and 3) to provide a parametrization of k_1 suitable for modeling R1 throughout the atmosphere, thereby reducing uncertainty in this important rate coefficient.

2. EXPERIMENTAL SECTION

The technique of Pulsed-Laser-Photolysis, Laser-Induced Fluorescence setup (PLP-LIF) was employed to determine the rate coefficients for the title reaction under pseudo-first-order conditions where [NO] exceeds [OH] by at least 2 orders of magnitude. The concentration of NO was calculated via manometric methods using accurately diluted gas mixtures. Optical absorption cells were used to monitor potential NO_2 and HONO impurities in NO mixtures and to measure [H_2O] in the experiments using H_2O-N_2 bath gas.

2.1. PLP-LIF Technique. The details of the PLP-LIF setup used in these experiments have been documented in previous publications,[13,38] and thus, only a brief description is provided here. The reactions took place in a jacketed, cylindrical quartz reactor with a volume of ∼500 cm^3 the temperature of which was controlled by circulating a 60:40 ethylene glycol−water mixture through an outer jacket. The temperature at the center of the reactor was measured by inserting a J-type thermocouple before and after each experiment. The pressure in the reactor and optical absorption cells (see below) was monitored by capacitance manometers (MKS) with ranges of 100 and 1000 Torr (1 Torr = 1.333 hPa). The experimental pressure was adjusted by varying the total flow rate and pumping speed. The total volume flow rate was varied to maintain an average linear velocity of ∼8−9 cm s^{-1} in the reactor at all experimental temperatures/pressures. The linear velocity at the center of the flow is likely to be larger (by up to a factor of 2 for laminar flow) than 8−9 cm s^{-1}, and as the 0.8 mm diameter laser beam propagates at right angles to the gas flow, we can be certain that photolysis occurs in a fresh gas mixture at each laser pulse (operated at 10 Hz).

OH radicals were generated by photolyzing H_2O_2 (R3) at a wavelength of 248 nm using a KrF excimer laser (COMPex 205F, Coherent).

$$H_2O_2 + h\nu\ (248\ nm) \rightarrow 2OH \qquad (R3)$$

OH radicals were excited at 282 nm ($A^2\sum$ (ν = 1) ← $X^2\Pi$ (ν = 0)) by a YAG-pumped dye laser, and the subsequent OH fluorescence was detected by a photomultiplier screened by a 309 nm interference filter and a BG 26 glass cutoff filter. The delay between the triggers of the photolysis and probe lasers was scanned using a digital delay generator. Time-dependent OH profiles (one laser pulse per data point) were obtained by accumulating the fluorescence signals using a boxcar integrator; 20−50 successive profiles were averaged to improve the signal-to-noise ratio. The photolysis laser fluence was measured by a joule meter placed behind the exit window of the reactor, and the shot-to-shot variation in the intensity of the dye laser was monitored by a photodiode. Each OH decay profile was composed of 20 points before the excimer laser was triggered (to determine the background signal) and 100 points after the trigger of the excimer laser for use in deriving the decay kinetics.

2.2. Online Optical Absorption Measurements. In our previous studies of atmospherically important, termolecular reactions involving the OH radical,[13,15] the concentrations of the excess reactants (SO_2 and NO_2) were accurately measured through in situ optical absorption techniques. NO displays several resolved absorption features in the VUV[39] but the more accessible features at 205, 215, and 226 nm are weak and do not coincide with the wavelengths of the atomic line sources available (Hg lines at 185, 254, and 365 nm or Zn at 214 nm)

https://doi.org/10.1021/acs.jpca.2c02369
J. Phys. Chem. A 2022, 126, 3863−3872

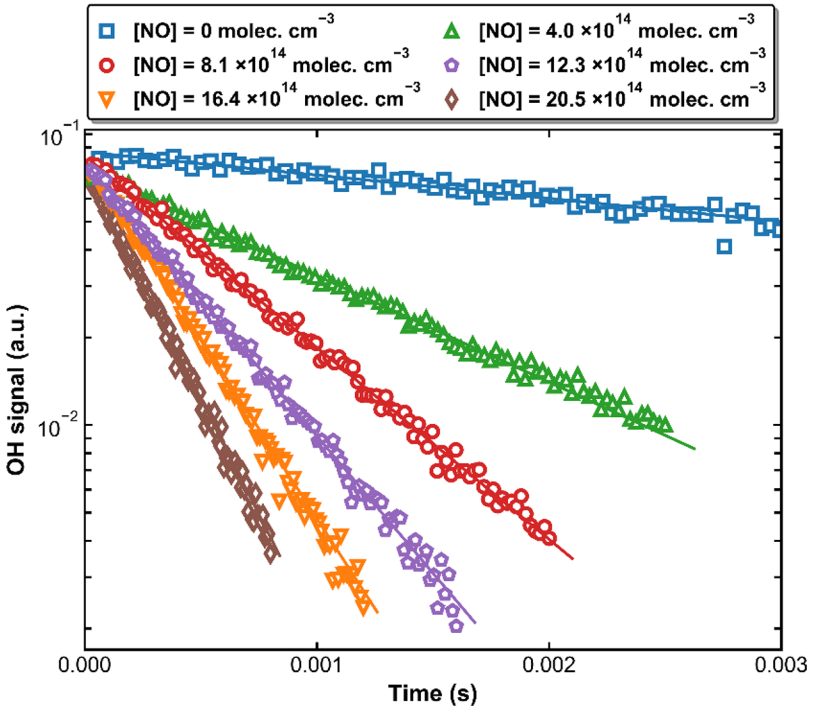

Figure 2. Exponential decay of the OH LIF signal in an experiment at 101.6 Torr N_2 at 298 K and six different [NO]. The solid lines are the fits to the data using eq 1.

or over the wavelength range (~230−700 nm) covered by our long-path absorption cell equipped with halogen and deuterium lamps. Compared to NO_2 and SO_2, which have affinity for surfaces, NO is easy to handle and has no losses in flow controllers, and diluted samples can be prepared with high accuracy. In this study, the concentration of NO was derived from its partial pressure in a supply canister, its partial flow rate into the reactor, and the total pressure and temperature. The mass flow controllers were freshly calibrated using a Gilibrator.

The purity of the NO sample was checked using an optical absorption cell (l = 110 cm) located upstream of the reactor. Light from a deuterium lamp was passed through the cell 8 times (resulting in an optical length of 880 cm) and detected by a low resolution ($\Delta\lambda$ = 2 nm) spectrograph (Ocean-Optics USB 2000). Absorption measurements between 250 and 600 nm were inspected for absorption features from NO_2 and HONO. The minimum absorbance that could be detected was 5×10^{-4} at 420 nm, which, using a cross section of 6×10^{-19} cm^2 molecule^{-1}[40] for NO_2 implies a maximum concentration of 2×10^{12} molecules cm^{-3}. This is a factor >100 less than the concentration of NO typically used in the experiments ($3-20 \times 10^{14}$ molecules cm^{-3}) and (as the rate coefficients for reaction with OH are similar) implies that NO_2 impurity does not significantly bias the loss of OH. Similarly, the characteristic absorption features of HONO at 354, 368, and 384 nm[41] were not observed, and an upper limit to its concentration could be established, once again excluding a significant bias to the data as a result of the reaction of OH with HONO.

A second (single-pass) optical absorption cell (l = 34.8 cm) equipped with a low-pressure 185 nm Hg lamp was located downstream of the reactor to measure water concentrations in the experiments using N_2-H_2O bath gases. An absorption cross section of $\sigma_{H_2O}(185\ \text{nm}) = 7.14 \times 10^{-20}$ cm^2 molecule^{-1}[42] was used to retrieve water concentrations, with the pressure and temperature difference between the reactor and the 185 nm cell taken into consideration.

2.3. Chemicals. Nitrogen (N_2, 99.999%) was supplied by Air Liquide and used without further purification. Hydrogen peroxide (H_2O_2, AppliChem, 35%) was vacuum distilled to >90 wt % purity. Distilled water (Merck, liquid chromatography grade) was degassed before use. Two different $NO-N_2$ mixtures were used for the experiments: one commercial mixture (nominal mixing ratio of 5%) was supplied by Air Liquide, and the other was self-made with 2.75 ± 0.05% NO. The self-made mixture was made using NO (99.9%, purchased from Air Liquide) following fractional distillation to remove impurities such as NO_2 and other nitrogen oxides. The uncertainty in the mixing ratio is based on a conservative estimate of the accuracy of pressure gauges used to make the mixture.

3. RESULTS AND DISCUSSION

3.1. Rate Coefficients (k_1) in N_2. Rate coefficients for the title reaction in N_2 were measured at three different temperatures (273, 298, and 333 K) over the pressure range of 22−743 Torr. In all experiments, the OH concentrations were kept sufficiently low (at the level of $10^{11}-10^{12}$ molecules cm^{-3}) in comparison to [NO] ($3-20 \times 10^{14}$ molecules cm^{-3}) to satisfy pseudo-first-order conditions so that the OH decay could be described by

$$[\text{OH}]_t = [\text{OH}]_0 \exp(-k't) \quad (1)$$

where $[\text{OH}]_0$ and $[\text{OH}]_t$ are the OH concentrations at time 0 and t, respectively, after the photolysis laser pulse. k' (in s^{-1}) is the pseudo-first-order rate coefficient defined as

$$k' = k_1[\text{NO}] + k_d \quad (2)$$

where k_1 is the bimolecular rate coefficient (in molecules cm^{-3}), and k_d (in s^{-1}) accounts for OH removal through

https://doi.org/10.1021/acs.jpca.2c02369
J. Phys. Chem. A 2022, 126, 3863−3872

diffusion out of the reaction zone and reaction with H_2O_2. Figure 2 presents exemplary OH decay profiles at 298 K at different [NO] at a total pressure of ~100 Torr N_2. The OH LIF signals decay exponentially, and the fits to eq 1 yield the corresponding values of k'. Figure 3 plots k' versus [NO] at four different pressures; k_1 is derived from the linear regression of k' versus [NO] according to eq 2. Values of k_1, together with the statistical (2σ) standard errors, are summarized in Table 1, in which the experimental conditions are also provided. We estimate the potential systematic error (mainly in [NO]) as <5% as the NO−N_2 mixture was prepared as precisely as possible, and all the flow controllers were calibrated prior to the experiments. Overall, an uncertainty of 8% was estimated for k_1.

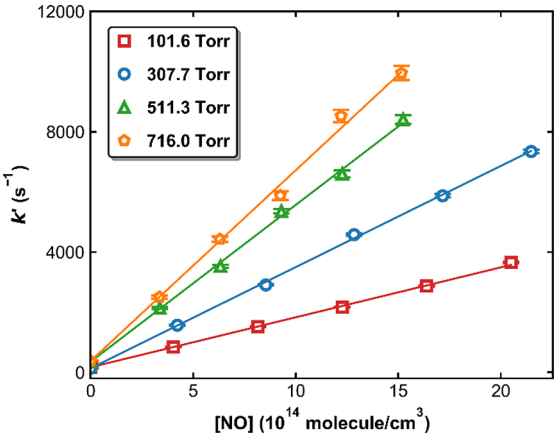

Figure 3. Pseudo-first-order rate coefficients (k') as a function of [NO] at 298 K and four different pressures. The error bars represent 2σ statistical uncertainties. The solid lines are linear regressions according to eq 2.

As mentioned in the Experimental Section, two NO−N_2 mixtures were used for the measurements. The first set of experiments was carried out using the bottled, commercial mixture, and the second set was carried out using our self-made mixture. The commercial mixture was not a primary standard, and thus the mixing ratio of NO was not sufficiently well-known to derive accurate rate coefficients. To obtain the exact NO concentration in the commercial (nominally 5%) mixture, measurements were performed under identical conditions using the two mixtures. Values of (k'-k_d), are plotted as a function of [NO] in Figure 4(a), in which the closed and open symbols represent measurements using the self-made and the commercial mixtures, respectively. The solid lines are the linear regressions for the (k'-k_d) measurements (in s^{-1}) with the self-made 2.75% NO mixture, which lie consistently above the data points obtained using the commercial mixture, indicating that the true NO concentration in the Air Liquide bottle should be lower than the nominal value. By systematically varying the mixing ratio of the commercial sample (using correction factors between 1 and 1.2) and refitting the data, we derived the best fit to the entire data set (i.e., the minimum standard deviation in the difference between the open symbols and solid lines in Figure 4). As shown in Figure 5, a correction factor of 1.086 (i.e., the true NO mixing ratio in the commercial sample is 4.60%) gives the best result. Figure 4(b) plots (k'-k_d) for all data obtained under identical conditions (both NO samples) when this correction is applied.

Figure 6 displays values of k_1 measured in N_2 bath gas as a function of the N_2 concentration (N_2 pressure was 22−744 Torr) at three different temperatures (273, 298, and 333 K). The solid lines are global, least-squares fits according to the Troe formalism[12] for termolecular reactions

$$k_1(T,p) = \frac{k_{1,0}^{N_2}\left(\frac{T}{300\text{K}}\right)^{-n}[M]k_{1,\infty}\left(\frac{T}{300\text{K}}\right)^{-m}}{k_{1,0}^{N_2}\left(\frac{T}{300\text{K}}\right)^{-n}[M] + k_{1,\infty}\left(\frac{T}{300\text{K}}\right)^{-m}}F \quad (3)$$

where $k_{1,0}^{N_2}$ (in cm^6 $molecule^{-2}$ s^{-1}) and $k_{1,\infty}$ (in cm^3 $molecule^{-1}$ s^{-1}) are the high-pressure and low-pressure limiting rate coefficients, respectively; T is the temperature in Kelvin; $[M]$ is the molecular density in molecules cm^{-3}; and n and m are dimensionless temperature exponents. The broadening factor F accounts for the lower rate coefficients in the fall-off regime compared to predictions by the Lindemann−Hinshelwood mechanism and is expressed as

$$\log F = \frac{\log F_C}{1 + \left[\log\left(\frac{k_{1,0}^{N_2}\left(\frac{T}{300\text{K}}\right)^{-n}[M]}{k_{1,\infty}\left(\frac{T}{300\text{K}}\right)^{-m}}\right)/N\right]^2} \quad (4)$$

where $N = 0.75-1.27 \log F_C$, and F_C is the broadening factor at the center of the fall-off curve.

To reduce the number of fit variables, and also because a relatively small temperature range is covered by the current measurements, we fix $k_{1,\infty}$ and its temperature dependence to values obtained in experiments in He at pressures up to 150 bar[28] that indicated that $k_{1,\infty}$ is ~3×10^{-11} cm^3 $molecule^{-1}$ s^{-1} with the temperature dependence (m = 0.3) derived from measurements at 250, 298, and 400 K.[30] Hence, only the parameters $k_{1,0}^{N_2}$, its temperature dependence (n), and F_C are allowed to vary.

The results are summarized in Figure 6 (solid lines) and in Table 2 where we also list the values preferred by IUPAC and NASA. In the Supporting Information, we also list and discuss the results obtained when different (or no) constraints to the fits are used. In summary, the fits obtained when fixing $k_{1,\infty}$ or when freely varying all parameters are of similar quality. However, the values of $k_{1,\infty}$, derived by freely varying all parameters are significantly lower than the results of high pressure experiments and have a strong negative temperature dependence, which reflects the fact that our data (in the fall-off region) do not define the high-pressure limiting rate coefficient well. The value of $k_{1,0}^{N_2} = 7.24 \times 10^{-31}$ $(T/300\text{ K})^{-2.17}$ cm^6 $molecule^{-2}$ s^{-1} that we obtain is in good agreement with those preferred by IUPAC and NASA (see Table 2), although the value of F_C = 0.53 is substantially lower than the calculated value of 0.81. We note that fixing F_C to 0.81 and using the IUPAC parameters for $k_{1,\infty}$ and m preclude a good fit to our data set (see discussion in the SI).

3.2. Comparison with Previous Measurements and Parametrizations for N_2 Bath Gas. Figure 7 presents a comparison of the present and previous measurements of k_1 in N_2 at around 298 K, our parametrization (Table 3) and the IUPAC and NASA evaluations at the same temperature.

Over the fall-off regime, most literature data sets obtained in N_2 were obtained at pressures well below 1 bar.[22,23,27,29] The current measurements and parametrization agree well with the data from Anastasi and Smith[23] and Donahue et al.,[29] while the data sets reported in Overend et al.[22] and Sharkey et al.[27] lie slightly below and above our measurements, respectively, at

https://doi.org/10.1021/acs.jpca.2c02369
J. Phys. Chem. A 2022, 126, 3863−3872

Table 1. Values of k_1 Measured in N_2 Bath Gas[a]

T (K)	p (Torr)	[M]	flow rate (SCCM)	[NO]	k_1	NO mixture
273	28	0.99	295	3.12–15.86	0.88 ± 0.02	b
273	49.1	1.74	452	2.98–13.51	1.39 ± 0.03	a
273	49.1	1.74	454	3.55–18.04	1.40 ± 0.05	b
273	74.6	2.64	688	3.56–18.08	1.92 ± 0.06	b
273	98.7	3.49	893	3.63–18.45	2.30 ± 0.05	b
273	124.4	4.40	1220	3.35–17.02	2.67 ± 0.03	b
273	153.3	5.42	1406	3.58–18.20	3.06 ± 0.05	b
273	199.4	7.05	1777	3.68–18.72	3.50 ± 0.16	b
273	248.3	8.78	2148	3.79–19.29	4.02 ± 0.08	b
273	306.7	10.85	2538	3.32–15.02	4.54 ± 0.25	a
273	306.7	10.85	2540	3.96–20.15	4.57 ± 0.18	b
273	353.8	12.51	3010	3.23–14.61	5.12 ± 0.16	a
273	411.3	14.54	3371	3.35–15.17	5.58 ± 0.21	a
273	511.4	18.08	4203	3.34–15.13	6.21 ± 0.25	a
273	608.1	21.50	5033	3.32–15.02	6.84 ± 0.20	a
273	714	25.25	5892	3.33–15.06	7.42 ± 0.23	a
298	22.2	0.72	182	3.03–13.86	0.53 ± 0.04	a
298	35.2	1.14	307	3.48–17.55	0.79 ± 0.03	b
298	50.2	1.63	436	3.46–17.58	1.00 ± 0.03	b
298	50.2	1.63	435	2.90–13.14	1.00 ± 0.01	a
298	61.3	1.99	504	3.66–18.60	1.20 ± 0.02	b
298	71.4	2.31	621	2.88–13.09	1.32 ± 0.02	a
298	100.2	3.25	821	3.07–13.90	1.79 ± 0.05	a
298	101.6	3.29	990	3.71–18.87	1.80 ± 0.05	b
298	121.2	3.93	1020	2.99–13.53	2.00 ± 0.03	a
298	148.6	4.81	1284	2.88–13.13	2.28 ± 0.08	a
298	205.9	6.67	1652	3.12–14.19	2.83 ± 0.03	a
298	253	8.20	2016	5.75–20.93	3.20 ± 0.34	a
298	305.9	9.91	2378	3.24–14.65	3.73 ± 0.21	a
298	307.7	9.97	2380	3.89–19.77	3.65 ± 0.14	b
298	407.5	13.20	3100	3.31–14.97	4.51 ± 0.16	a
298	511.3	16.56	3823	3.37–15.23	5.22 ± 0.32	a
298	614	19.89	4426	3.40–15.38	5.88 ± 0.06	a
298	716	23.19	5388	3.35–15.15	6.34 ± 0.47	a
333	26.9	0.78	235	3.09–15.68	0.43 ± 0.01	b
333	26.9	0.78	232	2.59–11.80	0.43 ± 0.04	a
333	39.4	1.14	275	3.86–19.63	0.58 ± 0.01	b
333	48.6	1.41	394	3.32–16.86	0.68 ± 0.02	b
333	48.6	1.41	392	2.78–12.64	0.71 ± 0.02	a
333	74.7	2.17	594	3.39–17.21	0.97 ± 0.02	b
333	100.6	2.92	753	3.59–18.27	1.28 ± 0.08	b
333	124.9	3.62	963	3.49–17.74	1.52 ± 0.04	b
333	145.9	4.23	1245	3.15–16.03	1.67 ± 0.04	b
333	198.4	5.75	1615	2.77–12.52	2.05 ± 0.06	a
333	198.8	5.76	1627	3.29–16.72	2.05 ± 0.09	b
333	248	7.19	2008	3.32–16.89	2.48 ± 0.10	b
333	303.3	8.79	2277	3.00–13.57	3.02 ± 0.09	a
333	407.3	11.81	3029	3.03–13.71	3.66 ± 0.13	a
333	502.7	14.57	3742	3.03–13.69	4.43 ± 0.28	a
333	616.2	17.86	4486	3.10–14.00	4.88 ± 0.25	a
333	743.8	21.56	5241	3.20–14.46	5.54 ± 0.20	a

[a]Units of [M] are 10^{18} molecules cm^{-3}. Units of k_1 are 10^{-12} cm^3 $molecule^{-1}$ s^{-1}. Units of [NO] are 10^{14} molecules cm^{-3}. The given total flow rates are calibrated values. Mixtures "a" and "b" are the self-made NO–N_2 mixture and the 5% NO in the N_2 mixture supplied by Air Liquide, respectively.

pressures >100 Torr. We further compared our parametrized rate coefficients to literature data obtained at temperatures beyond the current experimental range of 273–333 K. Data has been reported at 233 and 405 K (Anastasi and Smith[23]) and 216 K (Sharkey et al.[27]), and both our new parametrization and the NASA evaluation reproduce the measurements of k_1 at 233 and 405 K, while the IUPAC parametrization results in higher values, especially at 233 K (Figure S6). The rate coefficients reported by Sharkey et al.[27] at 216 K are larger than the parametrized rate coefficients, and their values at 298 K are also larger than reported in all other data sets (see Figure 7), which indicates a systematic bias related to their determination of the NO concentration.

Figure 7 (and Figure S5) shows that the parametrization derived in this work converges with those of the evaluation panels, particularly NASA, at low pressures.[23,27,29] Values of $k_{1,0}$ derived at low pressures using the discharge flow technique[19−21,24] vary greatly (from 5.8 × 10^{-31} to 15 × 10^{-31} cm^6 $molecule^{-2}$ s^{-1}) which might be related to experimental difficulties including, e.g., correcting for OH wall losses and axial diffusion, and these data are not represented in Figure 7.

https://doi.org/10.1021/acs.jpca.2c02369
J. Phys. Chem. A 2022, 126, 3863−3872

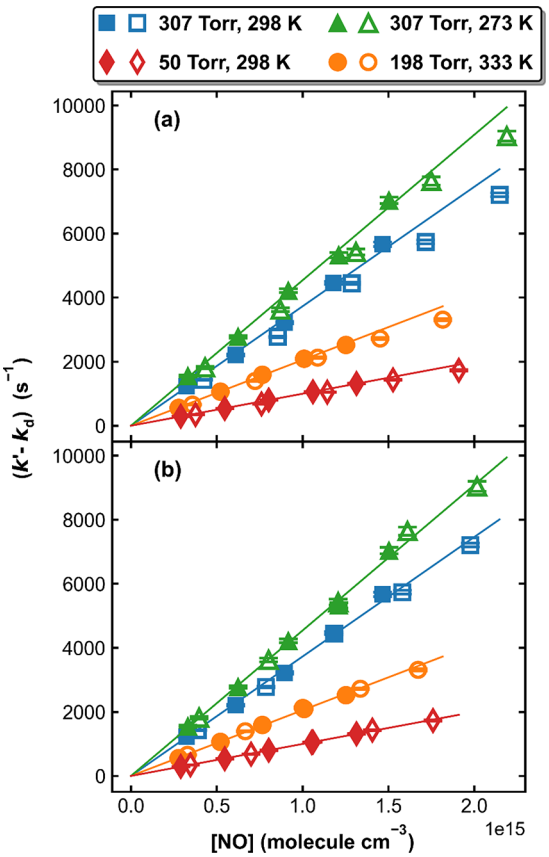

Figure 4. Measured values of (k'-k_d) as a function of [NO] using the self-made mixture (closed symbols) and the commercial mixture (open symbols) under four different experimental conditions. The solid lines are linear regressions of measurements with the self-made mixture. The NO mixing ratio is 5% in (a) and corrected to 4.60% in (b).

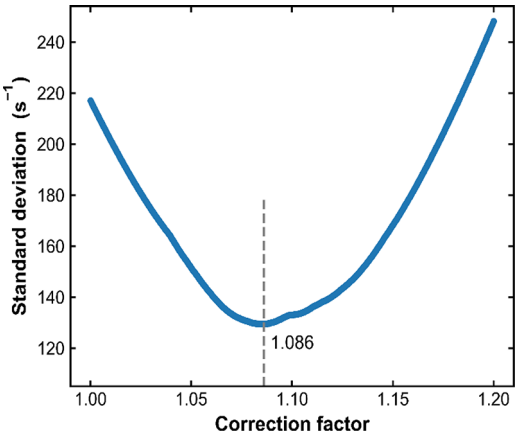

Figure 5. Standard deviation for the difference between the (k'-k_d) measurements with the commercial (nominal 5%) NO mixture (the open symbols in Figure 4) and the linear regressions (solid lines in Figure 4) through data points obtained with the self-made NO mixture as a function of the correction factor for the NO mixing ratio in the commercial sample.

3.3. Influence of Water Vapor on k_1.

Two recent publications from this group on termolecular reactions of OH indicated that H_2O is a very efficient collision partner compared to N_2.[14,15] We therefore measured k_1 in N_2−H_2O bath gases at a total pressure of 50 Torr and three different temperatures (273, 298, and 333 K). The relatively low pressure was chosen to best separate the contributions of H_2O and N_2 and remains far from the limiting high pressure regime. The H_2O mixing ratio x_{H_2O}, defined as the molar fraction of H_2O in the N_2 bath gas, was varied, and the corresponding values of k_1 were measured. x_{H_2O} was kept below 10% at 273 K

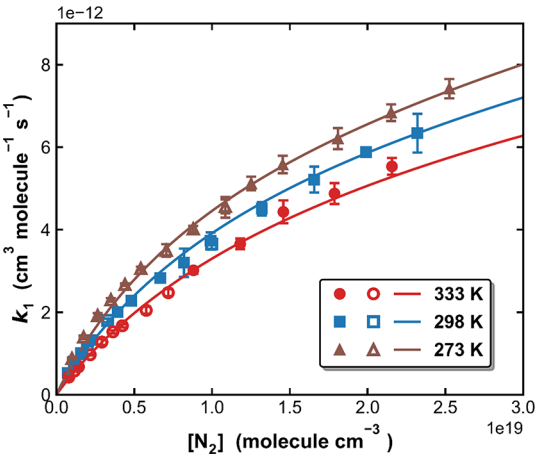

Figure 6. Measured k_1 (symbols) as a function of [N_2] at 273, 298, and 333 K in this work. The closed and open symbols represent measurements using the self-made and the Air Liquide mixtures, respectively. The solid lines are the fits (*Method 4*) of experimental data to eqs 3 and 4 with $k_{1,0}^{N_2}$ = 7.24 × 10^{-31} cm^6 $molecule^{-2}$ s^{-1}, n = 2.17, $k_{1,\infty}$ = 3.30 × 10^{-11} cm^3 $molecule^{-1}$ s^{-1}, m = 0.3, and F_C = 0.53.

Table 2. Parametrization of k_1 in N_2

	$k_{1,0}^{N_2}$ [a]	n	$k_{1,\infty}$ [b]	m	F_C	temp (K)
this work	7.24	2.17	**3.3**	**0.3**	0.53	273−333
IUPAC	7.4	2.4	3.3	0.3	0.81	200−400
NASA[c]	7.1	2.6	3.6	0.1	0.6	--

[a]Units of 10^{-31} cm^6 $molecule^{-2}$ s^{-1}. [b]Units of 10^{-12} cm^3 $molecule^{-1}$ s^{-1}. [c]The simplified form of the Troe expression for termolecular reactions used by NASA can be found in the Supporting Information. Numbers in bold type were fixed during fitting.

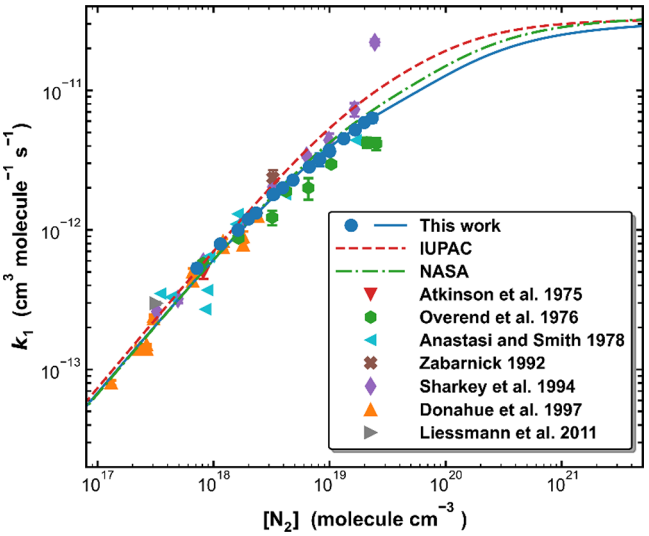

Figure 7. A comparison of measured and parametrized values of k_1 in N_2 bath gas at 298 K. The lines are values of k_1 derived from the parametrizations presented in this work (*Method 4*) and those by the IUPAC and NASA data-evaluation panels.

https://doi.org/10.1021/acs.jpca.2c02369
J. Phys. Chem. A 2022, 126, 3863−3872

Table 3. Values of k_1 Obtained in N_2−H_2O Bath Gases

T (K)	p (Torr)	M[a]	$[H_2O]$[b]	x_{H_2O}	x_{N_2}	k_1[c]
273	50.0	1.77	0.00	0.000	1.000	1.30 ± 0.04
	50.3	1.78	0.24	0.013	0.987	1.37 ± 0.03
	50.4	1.78	0.44	0.024	0.976	1.43 ± 0.00
	49.9	1.76	0.77	0.044	0.956	1.49 ± 0.05
	50.4	1.78	0.95	0.054	0.946	1.52 ± 0.06
	50.2	1.77	1.17	0.066	0.934	1.69 ± 0.04
	50.1	1.77	1.43	0.081	0.919	1.72 ± 0.05
298	50.2	1.63	0.00	0.000	1.000	1.00 ± 0.03
	50.5	1.63	0.26	0.016	0.984	1.02 ± 0.01
	50.0	1.62	0.49	0.031	0.969	1.04 ± 0.01
	50.2	1.63	0.56	0.035	0.965	1.12 ± 0.04
	50.0	1.62	0.91	0.056	0.944	1.16 ± 0.02
	50.1	1.62	1.20	0.074	0.926	1.28 ± 0.03
	49.9	1.62	1.55	0.096	0.904	1.33 ± 0.08
	50.3	1.63	2.04	0.125	0.875	1.40 ± 0.06
	50.3	1.63	2.51	0.154	0.846	1.48 ± 0.06
	50.4	1.63	2.68	0.164	0.836	1.44 ± 0.03
	50.1	1.62	2.94	0.181	0.819	1.60 ± 0.05
	49.9	1.62	3.26	0.202	0.798	1.61 ± 0.13
	49.8	1.61	3.74	0.232	0.768	1.72 ± 0.05
	49.9	1.62	4.02	0.249	0.751	1.88 ± 0.12
333	49.8	1.44	0.00	0.000	1.000	0.71 ± 0.01
	49.9	1.45	0.37	0.026	0.974	0.78 ± 0.04
	49.6	1.44	0.82	0.057	0.943	0.84 ± 0.01
	49.8	1.44	1.17	0.081	0.919	0.92 ± 0.04
	50.4	1.46	1.54	0.105	0.895	0.94 ± 0.06
	50.3	1.46	2.10	0.144	0.856	1.00 ± 0.09
	50.0	1.45	2.60	0.180	0.820	1.06 ± 0.08
	50.3	1.46	3.06	0.210	0.790	1.10 ± 0.07
	50.0	1.45	3.35	0.232	0.768	1.21 ± 0.09

[a]Units are 10^{18} molecules cm^{-3}. [b]Units are 10^{17} molecules cm^{-3}. [c]Units are 10^{-12} cm^3 $molecule^{-1}$ s^{-1}

and 25% at 298 and 333 K to avoid condensation of water in any part of the reactor or optical cell. In all experiments, the fluctuation of the total pressure was <1% so that the resulting influence on the measured k_1 was less than 1%.

Figure 8 plots values of k' as a function of the NO concentration in four bath gases containing different amounts of water vapor at 298 K and documents an increase in the slope of the linear regression (i.e., in k_1), with the concentration of water. At the highest water vapor concentration used (2.9×10^{17} molecules cm^{-3}), k_1 increases by around 60% compared to the value obtained in pure N_2 at this pressure and temperature.

Values of k_1 obtained in N_2−H_2O bath gases at 50 Torr and at three different temperatures are plotted against x_{H_2O} in Figure 9. The increasing value of k_1 with x_{H_2O} indicates that H_2O is a more efficient third-body quencher than N_2 for the title reaction and the effect of water on k_1 is also dependent on the temperature (largest slope at the lowest temperature). To evaluate the role of water in OH + NO kinetics and to derive a parametrization for k_1, the following equations are used to analyze the data

$$k(T,p) = \frac{\left(x_{N_2}k_{1,0}^{N_2}\left(\frac{T}{300K}\right)^{-n} + x_{H_2O}k_{1,0}^{H_2O}\left(\frac{T}{300K}\right)^{-o}\right)[M]k_{1,\infty}\left(\frac{T}{300K}\right)^{-m}}{x_{N_2}k_{1,0}^{N_2}\left(\frac{T}{300K}\right)^{-n} + x_{H_2O}k_{1,0}^{H_2O}\left(\frac{T}{300K}\right)^{-o})[M] + k_{1,\infty}\left(\frac{T}{300K}\right)^{-m}}F \quad (5)$$

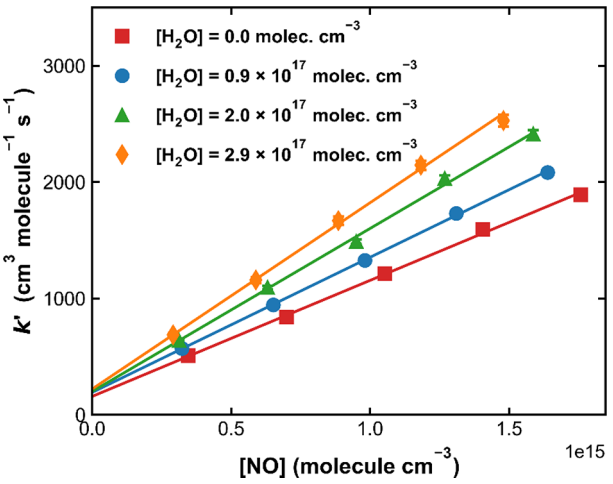

Figure 8. k' as a function of [NO] in N_2−H_2O bath gases with different water concentrations at 298 K and a total pressure of 50 Torr. The linear lines are the corresponding linear regressions.

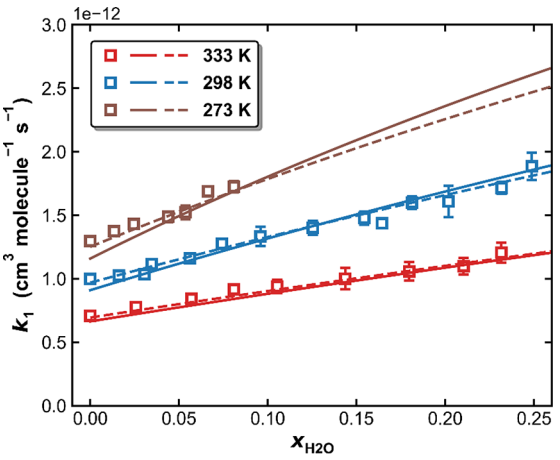

Figure 9. k_1 as a function of x_{H_2O} in N_2−H_2O bath gases at a total pressure of 50 Torr and three different temperatures. The symbols are measurements. The solid lines are fits to eq 5 and eq 6 with $k_{1,0}^{N_2}$, n = 2.17, $k_{1,\infty}$, m, and F_C constrained using parameters obtained in *Method 4* (Table S1). The resulting parameters in H_2O bath gas are $k_{1,0}^{H_2O}$ = 4.55×10^{-30} cm^6 $molecule^{-2}$ s^{-1} and o = 4.85. The dashed lines are the corresponding fits when using $k_{1,0}^{N_2}$, n = 2.17, $k_{1,\infty}$, m, and F_C constrained using parameters obtained in *Method 1* (Table S1). The resulting parameters in H_2O bath gas are $k_{1,0}^{H_2O}$ = 3.81×10^{-30} cm^6 $molecule^{-2}$ s^{-1} and o = 4.19.

where x_{H_2O} and x_{N_2} are the mole fractions of H_2O and N_2, $k_{1,0}^{H_2O}$ is the low-pressure limiting rate coefficient (cm^6 $molecule^{-2}$ s^{-1}) in pure H_2O, and o is a dimensionless temperature exponent. The broadening factor F is now defined as

$$\log F = \frac{\log F_C}{1 + \left[\log\left(\frac{x_{N_2}k_{1,0}^{N_2}\left(\frac{T}{300K}\right)^{-n} + x_{H_2O}k_{1,0}^{H_2O}\left(\frac{T}{300K}\right)^{-o})[M]}{k_{1,\infty}\left(\frac{T}{300K}\right)^{-m}}\right)/N\right]^2} \quad (6)$$

Equation 5 is essentially an extension of eq 3 in which the low-pressure limiting rate coefficients in N_2 and H_2O are linearly mixed. In eq 6, the same F_C is assumed for both N_2 and H_2O bath gases for simplification purposes.[14]

https://doi.org/10.1021/acs.jpca.2c02369
J. Phys. Chem. A 2022, 126, 3863−3872

Adopting the "dry" parameters obtained in pure N_2 ($k_{1,0}^{N_2}$, n, $k_{1,\infty}$, m, and F_C) using *Method 1* or *Method 4* (listed in the first and fourth row of Table S1), a global, least-squares fit to the N_2/H_2O data set results in $k_{1,0}^{H_2O} = 3.81 \times 10^{-30} (T/300\ K)^{-4.19}$ cm^6 $molecule^{-2}$ s^{-1} (*Method 1*, dashed lines in Figure 9) or $k_{1,0}^{H_2O} = 4.55 \times 10^{-30} (T/300\ K)^{-4.85}$ cm^6 $molecule^{-2}$ s^{-1} (*Method 4*, solid lines in Figure 9). While the differences in the fits obtained using *Method 1* and *Method 4* are slight at 333 and 298 K, the use of *Method 1* results in a poorer fit to the data at 273 K, which is (at least partially) due to the use of a larger value of k_∞. For the purpose of constraining the fit to the data of the H_2O-N_2 experiments, the accurate characterization of k_1 at low pressures is of primary importance, and the correct derivation of $k_{1,\infty}$ is less essential. As the rate coefficients at 50 Torr are far from $k_{1,\infty}$ and because the use of parameters obtained using *Method 1* to constrain the fit gives the best fit, we prefer $k_{1,0}^{H_2O} = 3.81 \times 10^{-30} (T/300\ K)^{-4.19}$ cm^6 $molecule^{-2}$ s^{-1}.

In both cases, it is clear that $k_{1,0}^{H_2O}$ (300 K) is a factor 5−6 larger than $k_{1,0}^{N_2}$ (300 K), similar to the results obtained in our studies of OH + NO_2 (+M) and OH + SO_2 (+M).[14,15]

Overend et al.[22] performed measurements in He−H_2O mixtures where the H_2O partial pressure ranged from 3 to 16 Torr over a total pressure of 20−30 Torr at 295 K. The results are displayed in Figure 10 which also plots our parametrized

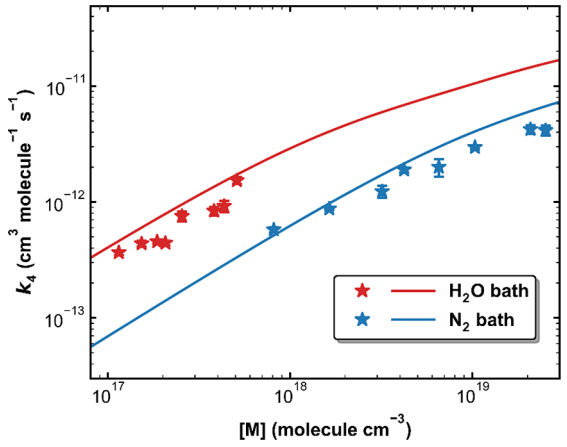

Figure 10. Fall-off curves for k_1 in H_2O and N_2 bath gases at 295 K. Solid lines are the current parametrizations based on *Method 4* (see Table S1). Symbols are measurements reported by Overend et al.[22]

fall-off curves for k_1 in pure H_2O and pure N_2 for comparison. In both bath gases, the current data and parametrizations lie above the rate coefficients reported by Overend et al.[22] whose data are significantly more scattered than those of the present study, which appears to stem from scatter in the plots of k' versus [NO]. Overend et al.[22] analyzed their data with a two-step Lindeman scheme and concluded that the collisional energy transfer efficiency of H_2O was a factor 8.3 greater than that of N_2, somewhat larger than the value of 5−6 derived in this work.

Liessmann et al.[37] addressed the role of H_2O in their studies of the title reaction in a Laval-nozzle expansion (61−135 K) at pressures close to 1 Torr and documented a significant increase in the rate coefficient (factors of 1.06 to 1.44) in the presence of H_2O (at 3% of the total pressure). Such a large enhancement in the rate coefficient in the presence of just 3% H_2O (i.e., $x_{H_2O} = 0.03$) is much greater than observed at the higher temperatures of the present study or than of Overend et al.[22] As discussed by Liessmann et al.,[37] the supersaturation of H_2O in the expansion favors cluster formation and the formation of $OH(H_2O)_n$, $NO(H_2O)_n$ prior to reaction, and also formation of the cluster $HONO(H_2O)_n$ may play a role in their experiments and explain the much larger effects they observed. In contrast to the Laval-nozzle experiments, low temperatures in the Earth's atmosphere are accompanied by low water−vapor mixing ratios, and the results obtained in the present study (and in that of Overend et al.[22]) are relevant for estimating the impact of considering (or, conversely, neglecting) the enhancement of k_1 in the presence of H_2O.

3.4. Implications for the Atmosphere. The discussion above indicates that H_2O is a much more efficient third-body quencher than N_2 for the NO + OH reaction, and a simple calculation serves to illustrate the impact of water vapor on the rate coefficient of the title reaction in the atmosphere. Consider the tropical boundary layer with a typical temperature of 30 °C (303 K), a total pressure of 1 bar (750 Torr), and a humidity of 100%. The major components (bath gases) of the air are 567 Torr N_2, 151 Torr O_2, and 32 Torr H_2O. We assume that O_2 has the same quenching efficiency as N_2, which is generally a very good approximation. Despite its lower concentration, the higher quenching efficiency of H_2O contributes more than O_2 to the collisional relaxation of HONO* (and thus the rate coefficient). The current parametrization yields values of k_1 (1 bar, 303 K) = 6.17×10^{-12} cm^3 $molecule^{-1}$ s^{-1} if the impact of H_2O is ignored and a >10% larger value of 6.86×10^{-12} cm^3 $molecule^{-1}$ s^{-1} when H_2O is considered (using $k_{1,0}^{H_2O} = 3.81 \times 10^{-30} (T/300\ K)^{-4.19}$ cm^6 $molecule^{-2}$ s^{-1}). At the same temperature and pressure, the parametrizations of the IUPAC and NASA panels (neither of which takes H_2O into account) result in values of 9.36×10^{-12} and 7.09×10^{-12} cm^3 $molecule^{-1}$ s^{-1}, respectively. The present data set and parametrization should be used to reassess the kinetic data for the title reaction and guide the IUPAC and NASA panels toward reaching consensus on their preferred values, especially at lower altitudes.

4. CONCLUSIONS

Rate coefficients of the title reaction NO + OH were measured at various temperatures and pressures (N_2) in the fall-off regime and used to develop a parametrization that accurately describes the present data and literature data sets even at temperatures outside the range of our measurements. Experiments in N_2-H_2O bath gases showed that water is a more efficient third-body quencher than N_2 by a factor of 5−6. The water effect was parametrized using a Troe type expression considering multiple bath gas components, which provides a comprehensive and reliable basis for atmospheric modeling.

■ ASSOCIATED CONTENT

Supporting Information

The Supporting Information is available free of charge at https://pubs.acs.org/doi/10.1021/acs.jpca.2c02369.

Description of fitting constraints (Methods 1−5) and associated figures (Figures S1−S4), comparison of k_1 with evaluations (Figures S5 and S6), NASA parametrization method for termolecular reactions, and parametrization of k_1 in N_2-H_2O bath gases using different values of F_C for N_2 and H_2O (PDF)

https://doi.org/10.1021/acs.jpca.2c02369
J. Phys. Chem. A 2022, 126, 3863−3872

AUTHOR INFORMATION

Corresponding Author

John N. Crowley − *Division of Atmospheric Chemistry, Max-Planck-Institute for Chemistry, 55128 Mainz, Germany;* orcid.org/0000-0001-8669-0230; Email: john.crowley@mpic.de

Authors

Wenyu Sun − *Division of Atmospheric Chemistry, Max-Planck-Institute for Chemistry, 55128 Mainz, Germany;* Present Address: Lawrence Livermore National Laboratory, CA, USA. Email: sun39@llnl.gov (W.S.)

Jos Lelieveld − *Division of Atmospheric Chemistry, Max-Planck-Institute for Chemistry, 55128 Mainz, Germany;* orcid.org/0000-0001-6307-3846

Complete contact information is available at: https://pubs.acs.org/10.1021/acs.jpca.2c02369

Funding

Open access funded by Max Planck Society.

Notes

The authors declare no competing financial interest.

ACKNOWLEDGMENTS

The research funding was provided by the Max Planck Society. Part of this work was performed under the auspices of the U.S. Department of Energy by Lawrence Livermore National Laboratory under Contract DE-AC52-07NA27344.

REFERENCES

(1) Crutzen, P. J. The role of NO and NO_2 in the chemistry of the troposphere and stratosphere. *Annu. Rev. Earth Planet. Sci.* **1979**, *7*, 443−472.

(2) Singh, H. B. Reactive nitrogen in the troposphere. *Environ. Sci. Technol.* **1987**, *21*, 320−327.

(3) Crutzen, P. J. Photochemical reactions initiated by and influencing ozone in unpolluted tropospheric air. *Tellus* **1974**, *26*, 47−57.

(4) Lightfoot, P. D.; Cox, R. A.; Crowley, J. N.; Destriau, M.; Hayman, G. D.; Jenkin, M. E.; Moortgat, G. K.; Zabel, F. Organic peroxy radicals - kinetics, spectroscopy and tropospheric chemistry. *Atmos. Environ., Part A* **1992**, *26*, 1805−1961.

(5) Wayne, R. P.; et al. The nitrate radical: Physics, chemistry, and the atmosphere. *Atmos. Env. A* **1991**, *25A*, 1−206.

(6) Wayne, R. P.; et al. Halogen oxides: Radicals, sources and reservoirs in the laboratory and in the atmosphere. *Atmos. Environ.* **1995**, *29*, 2677−2881.

(7) Wennberg, P. O.; et al. Removal of stratospheric O_3 by radicals: In situ measurements of OH, HO_2, NO, NO_2, ClO, and BrO. *Science* **1994**, *266*, 398−404.

(8) Meusel, H.; et al. Daytime formation of nitrous acid at a coastal remote site in Cyprus indicating a common ground source of atmospheric HONO and NO. *Atmos. Chem. Phys.* **2016**, *16*, 14475−14493.

(9) Elshorbany, Y. F.; Steil, B.; Brühl, C.; Lelieveld, J. Impact of HONO on global atmospheric chemistry calculated with an empirical parameterization in the EMAC model. *Atmos. Chem. Phys.* **2012**, *12*, 9977−10000.

(10) Meusel, H.; et al. Emission of nitrous acid from soil and biological soil crusts represents an important source of HONO in the remote atmosphere in Cyprus. *Atmos. Chem. Phys.* **2018**, *18*, 799−813.

(11) Ye, C.; Zhang, N.; Gao, H.; Zhou, X. Photolysis of Particulate Nitrate as a Source of HONO and NOx. *Environ. Sci. Technol.* **2017**, *51*, 6849−6856.

(12) Troe, J. Theory of thermal unimolecular reactions in the fall-off range 1. Strong collision rate constants. *Ber. Bunsen-Ges. Phys. Chem. Chem. Phys.* **1983**, *87*, 161−169.

(13) Amedro, D.; Bunkan, A. J.; Berasategui, M.; Crowley, J. N. Kinetics of the OH+ NO_2 reaction: rate coefficients (217−333 K, 16−1200 mbar) and fall-off parameters for N_2 and O_2 bath gases. *Atmos. Chem. Phys.* **2019**, *19*, 10643−10657.

(14) Amedro, D.; Berasategui, M.; Bunkan, A. J.; Pozzer, A.; Lelieveld, J.; Crowley, J. N. Kinetics of the OH+NO_2 reaction: effect of water vapour and new parameterization for global modelling. *Atmos. Chem. Phys.* **2020**, *20*, 3091−3105.

(15) Sun, W.; Berasategui, M.; Pozzer, A.; Lelieveld, J.; Crowley, J. Kinetics of OH + SO_2 + M: Temperature-dependent rate coefficients in the fall-off regime and the influence of water vapour. *Atmos. Chem. Phys.* **2022**, *22*, 4969−4984.

(16) Morley, C.; Smith, I. W. M. Rate measurements of reactions of OH by resonance absorption. 1. Reactions of OH with NO_2 and NO. *J. Chem. Soc., Faraday Trans.* **1972**, *68*, 1016−1030.

(17) Stuhl, F.; Niki, H. Flash Photochemical Study of the Reaction OH+NO+M Using Resonance Fluorescent Detection of OH. *J. Chem. Phys.* **1972**, *57*, 3677−3679.

(18) Westenberg, A. A.; Dehaas, N. Rate measurements on OH+NO +M and OH+NO_2+M. *J. Chem. Phys.* **1972**, *57*, 5375−5378.

(19) Anderson, J. G.; Margitan, J. J.; Kaufman, F. Gas-phase recombination of OH with NO and NO_2. *J. Chem. Phys.* **1974**, *60*, 3310−3317.

(20) Howard, C. J.; Evenson, K. M. Laser magnetic-resonance study of gas-phase reactions of OH with CO, NO, and NO_2. *J. Chem. Phys.* **1974**, *61*, 1943−1952.

(21) Harris, G. W.; Wayne, R. P. Reaction of hydroxyl radicals with NO, NO_2 and SO_2. *J. Chem. Soc. Faraday Trans. I* **1975**, *71*, 610−617.

(22) Overend, R.; Paraskevopoulos, G.; Black, C. Rates of OH radical reactions. II. The combination reaction OH+NO+M. *J. Chem. Phys.* **1976**, *64*, 4149−4154.

(23) Anastasi, C.; Smith, I. W. M. Rate measurements of reactions of OH by resonance absorption. Part 6.—Rate constants for OH + NO (+M)→ HNO_2 (+M) over a wide range of temperature and pressure. *J. Chem. Soc. Faraday Trans II* **1978**, *74*, 1056−1064.

(24) Burrows, J. P.; Wallington, T. J.; Wayne, R. P. Kinetics of the gas-phase reactions of OH with NO_2 and with NO. *J. Chem. Soc. Faraday Trans II* **1983**, *79*, 111−122.

(25) Zabarnick, S. Kinetics of the reaction OH + NO + M → HONO + M as a function of temperature and pressure in the presence of argon, SF_6, and N_2 bath gas. *Chem. Phys.* **1993**, *171*, 265−273.

(26) Atkinson, D. B.; Smith, M. A. Radical-molecule kinetics in pulsed uniform supersonic flows- Termolecular association of OH plus NO between 90 and 220 K. *J. Phys. Chem.* **1994**, *98*, 5797−5800.

(27) Sharkey, P.; Sims, I. R.; Smith, I. W. M.; Bocherel, P.; Rowe, B. R. Pressure and temperature dependence of the rate constants for the association reaction of OH radicals with NO between 301 and 23 K. *J. Chem. Soc., Faraday Trans.* **1994**, *90*, 3609−3616.

(28) Forster, R.; Frost, M.; Fulle, D.; Hamann, H. F.; Hippler, H.; Schlepegrell, A.; Troe, J. High pressure range of the addition of HO to HO, NO, NO_2, and CO. I. Saturated laser induced fluorescence measurements at 298 K. *J. Chem. Phys.* **1995**, *103*, 2949−2958.

(29) Donahue, N. M.; Dubey, M. K.; Mohrschladt, R.; Demerjian, K. L.; Anderson, J. G. High-pressure flow study of the reactions OH +NOx->HONOx: Errors in the falloff region. *J. Geophys. Res. -Atmos.* **1997**, *102*, 6159−6168.

(30) Fulle, D.; Hamann, H. F.; Hippler, H.; Troe, J. Temperature and pressure dependence of the addition reactions of HO to NO and to NO_2. IV. Saturated laser-induced fluorescence measurements up to 1400 bar. *J. Chem. Phys.* **1998**, *108*, 5391−5397.

(31) Pagsberg, P.; Bjergbakke, E.; Ratajczak, E.; Sillesen, A. Kinetics of the gas phase reaction OH + NO(+M)→HONO(+M) and the determination of the UV absorption cross sections of HONO. *Chem. Phys. Lett.* **1997**, *272*, 383−390.

(32) Atkinson, R.; Hansen, D. A.; Pitts, J. N. Rate constants for the reaction of the OH radical with H_2 and NO (M = Ar and N_2). *J. Chem. Phys.* **1975**, *62*, 3284−3288.
(33) Atkinson, R.; Baulch, D. L.; Cox, R. A.; Crowley, J. N.; Hampson, R. F.; Hynes, R. G.; Jenkin, M. E.; Rossi, M. J.; Troe, J. Evaluated kinetic and photochemical data for atmospheric chemistry: Volume I - gas phase reactions of O*x*, HO*x*, NO*x* and SO*x* species. *Atmos. Chem. Phys.* **2004**, *4*, 1461−1738.
(34) IUPAC Task Group on Atmospheric Chemical Kinetic Data Evaluation, (Ammann, M., Cox, R. A., Crowley, J. N., Herrmann, H., Jenkin, M. E., McNeill, V. F., Mellouki, A., Rossi, M. J., Troe, J., Wallington, T. J.). http://iupac.pole-ether.fr/index.html (accessed 2021-09).
(35) Burkholder, J.; Sander, S.; Abbatt, J.; Barker, J.; Cappa, C.; Crounse, J.; Dibble, T.; Huie, R.; Kolb, C.; Kurylo, M. *Chemical kinetics and photochemical data for use in atmospheric studies: evaluation number 19*; Jet Propulsion Laboratory, National Aeronautics and Space Administration: 2020.
(36) Burrows, J. P.; Wallington, T. J.; Wayne, R. P. Kinetics of the gas-phase reactions of OH with NO_2 and with NO. *J. Chem. Soc. Faraday Trans II* **1983**, *79*, 111−122.
(37) Liessmann, M.; Miller, Y.; Gerber, B.; Abel, B. Reaction of OH and NO at Low Temperatures in the Presence of Water: the Role of Clusters. *Z. Phys. Chem.* **2011**, *225*, 1129−1144.
(38) Wollenhaupt, M.; Carl, S. A.; Horowitz, A.; Crowley, J. N. Rate coefficients for reaction of OH with acetone between 202 and 395 K. *J. Phys. Chem. A* **2000**, *104*, 2695−2705.
(39) Thompson, B. A.; Harteck, P.; Reeves, R. R., Jr Ultraviolet absorption coefficients of CO_2, CO, O_2, H_2O, N_2O, NH_3, NO, SO_2, and CH_4 between 1850 and 4000 A. *J. Geophys. Res.* **1963**, *68*, 6431−6436.
(40) Vandaele, A. C.; Hermans, C.; Simon, P. C.; Carleer, M.; Colin, R.; Fally, S.; Merienne, M. F.; Jenouvrier, A.; Coquart, B. Measurements of the NO_2 absorption cross-section from 42 000 cm^{-1} to 10 000 cm^{-1} (238−1000 nm) at 220 and 294 K. *J. Quant. Spectrosc. Radiat. Transfer* **1998**, *59*, 171−184.
(41) Stutz, J.; Kim, E. S.; Platt, U.; Bruno, P.; Perrino, C.; Febo, A. UV-visible absorption cross sections of nitrous acid. *J. Geophys. Res.: Atmospheres* **2000**, *105*, 14585−14592.
(42) Cantrell, C. A.; Zimmer, A.; Tyndall, G. S. Absorption cross sections for water vapor from 183 to 193 nm. *Geophys. Res. Lett.* **1997**, *24*, 2195−2198.

https://doi.org/10.1021/acs.jpca.2c02369
J. Phys. Chem. A 2022, 126, 3863−3872